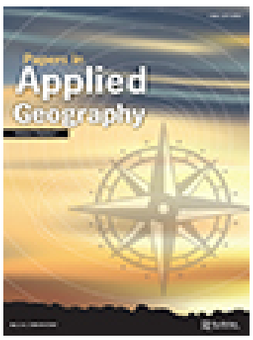

Papers in Applied Geography

ISSN: 2375-4931 (Print) 2375-494X (Online) Journal homepage: https://www.tandfonline.com/loi/rpag20

Detecting new building construction in urban areas based on images of small unmanned aerial system

Huan Ning, Xiao Huang, Zhenlong Li, Cuizhen Wang & Duowen Xiang

To cite this article: Huan Ning, Xiao Huang, Zhenlong Li, Cuizhen Wang & Duowen Xiang (2019): Detecting new building construction in urban areas based on images of small unmanned aerial system, Papers in Applied Geography, DOI: 10.1080/23754931.2019.1707108

To link to this article: https://doi.org/10.1080/23754931.2019.1707108

Published online: 27 Dec 2019.

PAPERS IN APPLIED GEOGRAPHY
https://doi.org/10.1080/23754931.2019.1707108

Detecting new building construction in urban areas based on images of small unmanned aerial system

Huan Ning[a,b], Xiao Huang[a], Zhenlong Li[a], Cuizhen Wang[a], and Duowen Xiang[c]

[a]Geoinformation and Big Data Research Laboratory, Department of Geography, University of South Carolina, Columbia, South Carolina, USA; [b]Wuhan Sunmap RS Co., Ltd., Wuhan, China; [c]Hi-Target Surveying Instrument Co., Ltd, Wuhan, China

ABSTRACT

The small Unmanned Aerial System (sUAS) is an emerging approach to monitor new buildings. sUAS acquires ultra-high-resolution imagery which provides visual evidence and reduces the necessity of in-situ investigation. It offers greater potential for building change detection when two epochs of images of the place of interest are captured. This study takes the entire urban area of Longfeng Town, Hubei Province, China as a test site, where two sets of 0.05 m resolution sUAS images were acquired on March 23, 2017 and June 6, 2017, respectively. In this short time interval, the heightened structures of the existing buildings consist of most changes. This study proposes a sensitive building change detection method by integrating the visual and elevation information from sUAS images. Dense point clouds were generated using sUAS images without control points. Two Digital Surface Models (DSM) are generated based on point clouds to detect elevation changes between two epochs. With true-color images, the improved Triangle Greenness Index (TGI) is used to mask out the natural changes caused by seasonal vegetation growth. Lastly, multiple criteria are utilized to identify changes in buildings including new buildings on the ground and new stories atop current buildings. The experimental result reveals that over 93.3% of building changes, including 3 new buildings and 25 stories and structures added to existing buildings are detected, which proves the validity of the proposed method for local land-use enforcement. The proposed method takes 5 minutes to extract changes from orthoimages and DSMs of 2 km^2, while manual monitoring is more than 40 times slower.

KEYWORDS

Building Change Detection; New Stories; Triangle Greenness Index (TGI); Digital Surface Model (DSM); Unmanned Aerial System (UAS)

Introduction

Buildings are the most essential structures in developed land. As a basic demand of people's living and business, building construction requires a strict regulation from the municipality. Meanwhile, the construction process is irreversible between land uses. For example, once farmland was occupied by buildings, the topsoil is removed or destroyed that cannot be restored for farming again in the human time scale (Maiti 2013). Therefore, local governments closely monitor urban land-use practices to ensure that the use of the precious nonrenewable land resource is appropriate, and building construction follows the urban planning policies (Champion et al. 2009; Matikainen et al. 2010).

CONTACT Zhenlong Li zhenlong@sc.edu Geoinformation and Big Data Research Laboratory, Department of Geography, University of South Carolina, Columbia, SC, USA.

However, in areas where effective government supervision and monitoring are lacking, for example, some rural areas in China, the areal or vertical sprawl of buildings often occurs illegally due to the high pressure of increasing population and increasing estate price (Weng 2002; Deng et al. 2009; Y. Liu, Fang, and Li 2014). A new building may illegally occupy farmland, or its height may exceed the planning permission. Field surveys are commonly adopted to identify illegal construction but are extremely labor-intensive and costly. In vast rural China, the authority needs a rapid and low-cost approach to ensuring the orderly conduct of urban construction.

Various studies have been conducted to detect new buildings using high-resolution remote sensing data (Hussain et al. 2013). Changed areas can be detected from two images captured in different periods (epochs) by overlaying new data on historical data (Stal et al. 2013; Tian, Cui, and Reinartz 2014; Szabó et al. 2016). In general, remote sensing data used for change detection can be categorized as 2-dimensional (2D, *e.g.*, optical images) and 3-dimensional (3D, with elevation involved). The 2D images provide rich visual and textural information that helps us label new buildings intuitively via photo interpretation. In the urban area, the abundant textural information in sUAS images imposes difficulties in detection algorithms (Hussain et al. 2013). In addition, slant images taken from satellite or airborne sensors contain the facades of high-rise buildings, making the building detection more challenging, especially in highly urbanized districts.

Some studies used elevation information to generate the DSM (Digital Surface Model) to detect vertical changes by comparing with existing data, such as house footprints (Champion 2007; L.-C. Chen and Lin 2010; Stal et al. 2013). DSMs are often derived from photogrammetric or LiDAR (Light Detection and Ranging) techniques. Photogrammetric methods use high-resolution image pairs based on stereoscopic vision principle to generate DSM. LiDAR directly measures the 3D coordinates of mass points on the earth surface, providing high vertical accuracy up to 0.15 meters (Baltsavias 1999; Hodgson and Bresnahan 2004; X. Liu 2011). However, LiDAR is generally less cost-effective and lacking visual evidence for verification. Some studies combined 2D and 3D data sources to improve accuracy (Ioannidis, Psaltis, and Potsiou 2009; Awrangjeb, Ravanbakhsh, and Fraser 2010; Hermosilla et al. 2011; L.-C. Chen and Lin 2010).

Small Unmanned Aerial System (sUAS), an emerging technology since the last decade (Colomina and Molina 2014), provides a user-controlled, cost-efficient approach of building change detection (Qin 2014; Unger, Reich, and Heipke 2014). Cameras equipped on sUASs can obtain 0.05-0.20 m ultra-high-resolution images, with less subjected to weather conditions than airborne or satellite sensors since data can be acquired under cloud cover. Most importantly, 3D products, such as dense point clouds and DSMs could be produced from sUAS images at lower costs than LiDAR and manned aerial photogrammetry (Sui et al. 2014; Kršák et al. 2016). Studies have been conducted on change detection based on sUAS images (Xuan 2011; R. Qin et al. 2015; B. Chen et al. 2016). However, to the best of our knowledge, little literature explicitly mentioned the detection of added stories or structures. If the monitoring period is within months, few new buildings will be completed from the ground up. Thus, the monitoring will fail to capture the building under construction. A method to detect the added stories or structures is needed.

In addition, most existing approaches need common ground control points (GCPs) to align sUAS images obtained in different periods (Shalaby and Tateishi 2007; Tong et al. 2012; Rongjun Qin, Tian, and Reinartz 2016). The GCPs need to be manually measured, which is a labor-intensive and error-prone process. Unger, Reich, and Heipke (2014) used sUAS images with a resolution of 2 cm and 18 GCPs with an accuracy of 2 cm to monitor a construction zone. They processed each epoch respectively and obtained the changes in DSMs between epochs. The authors manually analyzed changes of height and did not remove the un-wanted height differences (cars, containers, and people). According to the checkpoints, the RMS in the vertical direction is 2.9 to 5.2 cm, but the researchers reported a systematic error (>15 cm) in some unchanged buildings. Rongjun Qin (2014) and Li et al. (2017) achieved the detection of changed buildings

by registering the epochs of sUAS images in a single aero-triangulation procedure without GCPs. These two articles, however, do not provide an analysis of various situations in urban areas due to their rather small study areas (0.08 - 0.46 km2) with a small number of changes.

In this paper, we describe a method to detect new buildings and new constructions added on existing buildings in the entire urban area of a town in China using sUAS ultra-high-resolution images without GCPs. By combining the analyses of DSM and color information, building changes are detected with high recall. We also elaborate on the various false detection in the complex urban context which is not well recorded in most literature. The experimental result in the study area confirms that the heightened buildings consist of most building changes. The method proposed in this study could seed a wide range of studies in detecting those heightened buildings.

Materials and methods

Case description

The case study area is the entire urban area of Longfeng Town (109°30′33″E, 30°22′59″N), located in the west of Hubei Province, China (Figure 1). It covers approximately 2 km^2 with major land-use types of urban built-ups, farmlands, and forests. The elevation ranges from 440 to 530 m. Longfeng Town is close to Enshi City, the most economically developed city in the west of Hubei Province. The land source in this hilly region is scarce, and a large amount of illegal building has spread within the urban area.

The primary datasets used in this study include sUAS images were obtained at two different epochs. The fixed-wing sUAS was equipped with a true-color camera (SONY ILCE-7R, lens: 35 mm, pixel size: 0.00488 mm). The first epoch (Epoch A) took place at 5:00 PM March 23, 2017 with 408 images in a mission. Its endlap and sidelap are 70 percent and 40 percent, respectively. Conducted at 1:00 PM June 6, 2017, the second epoch (Epoch B) has 1,032 images with an endlap

Figure 1. The urban area (red box) of Longfeng Town in Hubei Province, China. The displayed image is the orthomap of the sUAS image on June 6, 2017.

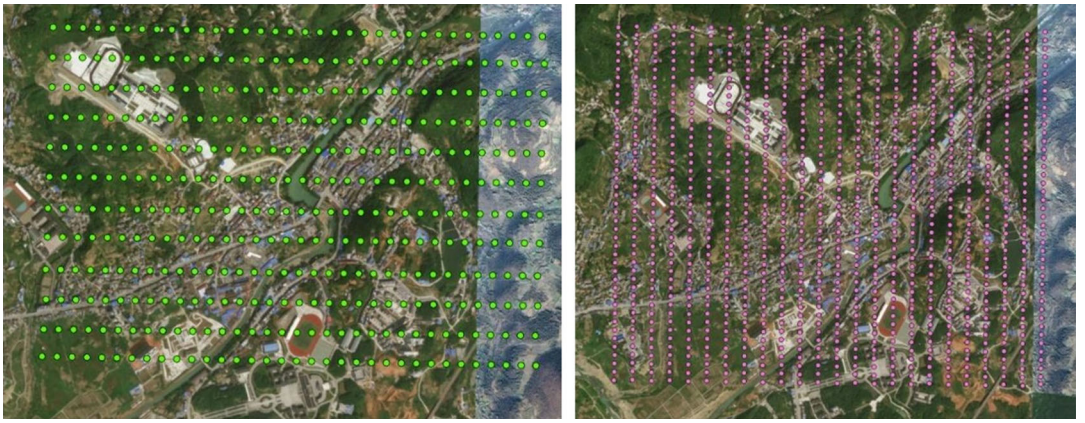

Figure 2. Photograph exposure stations of Epoch A (green dots) and B (purple dots).

of 80 percent and a sidelap of 50 percent, also obtained in a mission. Figure 2 shows the locations of images in two epochs. Epoch B was obtained in the early summer when vegetation has grown more leaves than Epoch A. Images from both epochs were acquired in sunny weather, at the vertical view at a flying height of 750 m. Each image contains 7,360 × 4,912 pixels with a resolution of 0.05 m. Epoch B has more images due to higher endlap and sidelap, which are compensation for the vibration from the stronger wind on that day.

Methodological design

The proposed approach includes: 1) conducting aero-triangulation for two epochs in a single project; 2) generating the DSM and True Digital Ortho Map (TDOM) of each epoch; 3) extracting changed areas based on differential DSM and Triangular Greenness Index (TGI), and 4) extracting changed buildings from the changed areas (Figure 3). After obtaining the DSMs and TDOMs, the subsequential workflow was implemented as a customized tool of ArcGIS Pro Toolbox (Figure 4). We manually labeled the changed buildings by photo interpretation to obtain the ground truth and performed an error assessment of sUAS-extracted building changes in the study area.

Single project aero-triangulation

The photogrammetric method was used to produce DSM and TDOM in this study. As an essential procedure in photogrammetry, aero-triangulation is a technique to calculate the sensor's position and orientation when a photograph was taken (Nex and Remondino 2014). We used PhotoScan 1.3 (Verhoeven 2011) to conduct the aero-triangulation. Considering that the two sets of images were acquired in a short time interval (2.5 months) using the same camera and the earth surface did not change much, we processed both image epochs in a single aero-triangulation project. No GCP was used in the aero-triangulation. When aligning photo in PhotoScan, we set "Accuracy" to "High", "Tie points limit" to "40,000", "Adaptive camera model fitting" to activate, and set "Quality" to "High", "Depth filtering" to "Aggressive" when generating DSMs.

Extraction of DSM and TDOM

After the aero-triangulation, the DSM and TDOM of each epoch (DSM_A, DSM_B, $TDOM_A$, and $TDOM_B$) were generated by PhotoScan. Then, the alignment of the two epochs of DSM and

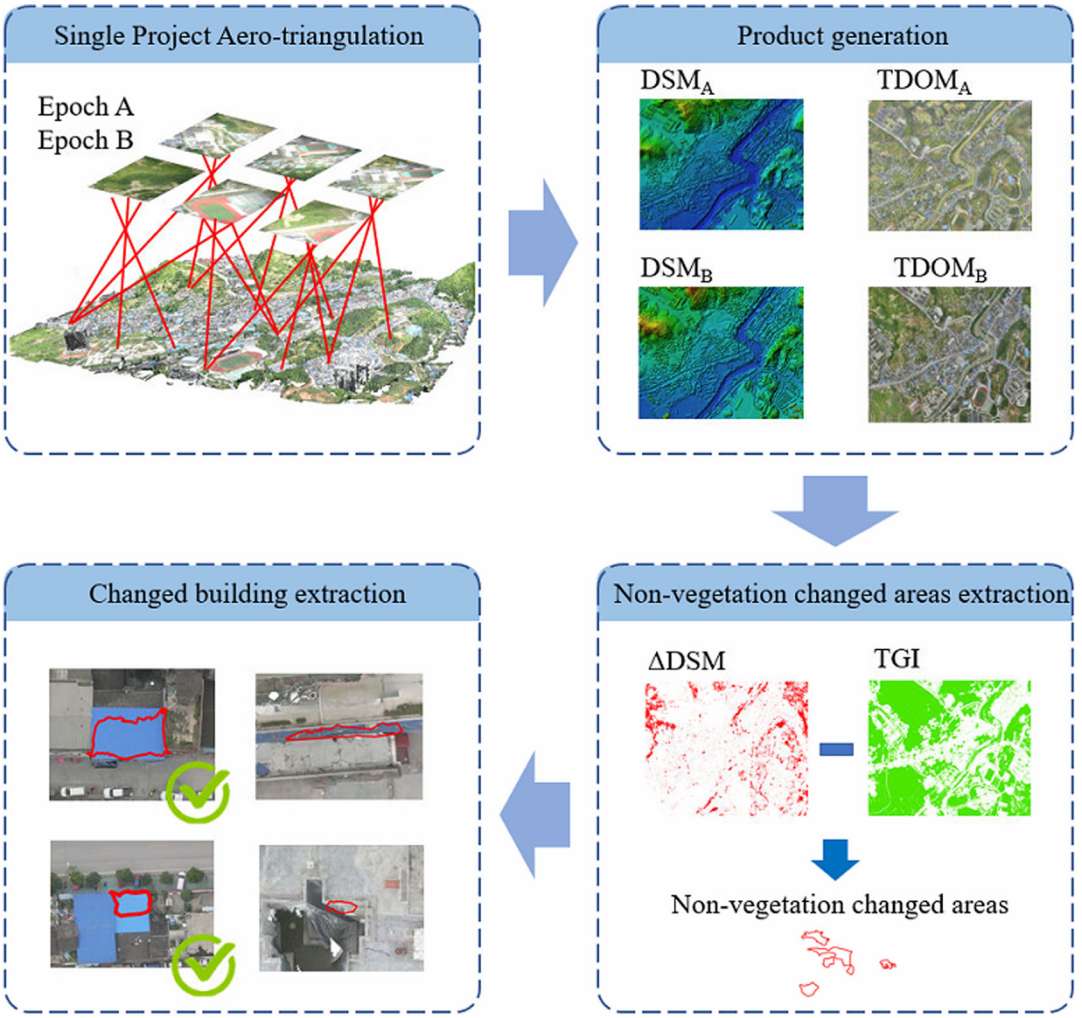

Figure 3. The overall workflow of the proposed method.

TDOM were assessed to see how large the change can be detected vertically and horizontally. We evenly selected 500 unchanged hard flat surfaces (*e.g.*, rooftop or road) in the study area to assess the vertical alignment between DSMs. Theoretically, the elevation in DSM_A and DSM_B should be the same in those unchanged areas. Thus, the differences between two DSMs (ΔDSM, which reveals height changes in two epochs) in unchanged areas indicate the error of the alignment. We used the average of pixel values of the unchanged surfaces in ΔDSM to indicate the error. To reflect added stories, the error of the DSMs should be much smaller than the height of a regular building story. Finaly, the pixels within 1 m interval of elevation changes were reclassified then converted to polygons. For example, pixels in ΔDSM between 0 – 1 m will be labeled as one class and will be converted to polygons. The adjacent pixels with similar values become a polygon, indicating a changed area.

Extraction of non-vegetation changes

Aside from new building construction, the height changes in the test site in two epochs are heavily affected by seasonal vegetation growth. With true-color sUAS images, we adopted the Triangular

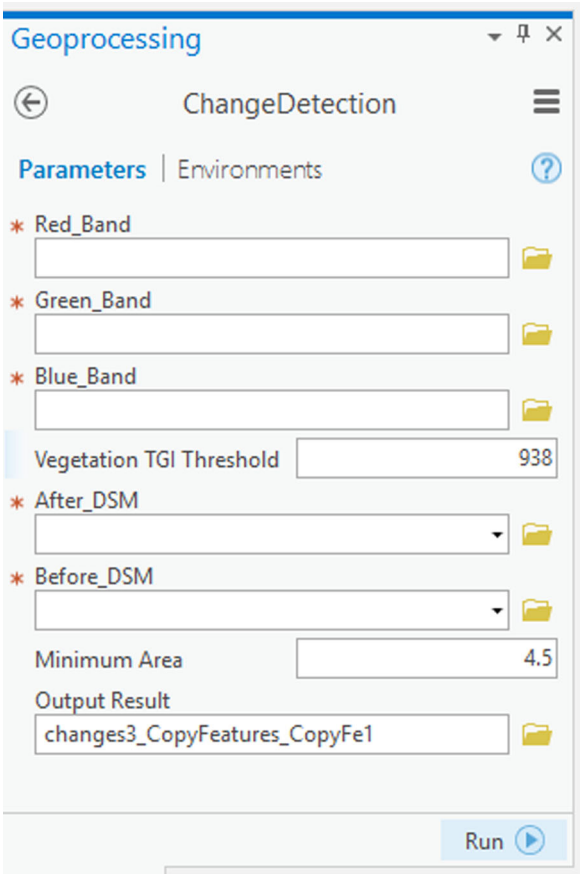

Figure 4. The customized change detection tool implemented in ArcGIS Pro Toolbox.

Greenness Index (TGI) (Hunt et al. 2013) to mask out vegetation. The remaining areas with DSM changes represent the non-vegetation changes. The TGI is a vegetation index that estimates leaf chlorophyll content relying on spectral reflectance in the visible spectrum (Hunt et al. 2013):

$$TGI = -0.5\left[(\lambda_r - \lambda_b)(R_{670} - R_{550}) - (\lambda_r - \lambda_g)(R_{670} - R_{480})\right] = 95R_{550} - 60R_{480} - 35R_{670} \quad (1)$$

Where R_{670}, R_{550} and R_{480} represent the reflectance in red, green and blue spectral regions, respectively; λ_r, λ_g, and λ_b represent their wavelengths. In this study, they were centered at 670 nm, 550 nm, and 480 nm for three bands of the sUAS camera. To simplify the process, we used the Digital Number (DN) values of the 8-bit sUAS imagery as the scaled reflectance in Equation (1).

Figure 5 demonstrates the DN (in R, G, and B bands) values and TGI using example pixels of several common land uses in the study area. For vegetation types (grass, tree, agriculture, and bush), Figure 5(a) reveals their distinctive triangular patterns with a high DN value in the green band. For non-vegetation types (Road, Rooftop, and Bareland), contrarily, Figure 5(b) and (c) show that they have much smaller areas of the triangle.

We statistically compared 214 vegetation sample sites to determine a TGI threshold between vegetation and non-vegetation in $TDOM_B$ (Figure 6). These sample sites were manually chosen and evenly distributed as possible in different vegetation zones. Vegetation types included trees, crops, and bushes, and their TGI histogram is presented in Figure 6(b). In general, these TGI values show a normal distribution pattern where the mean value, M_{tgi}, is 3061.96, and the standard deviation,

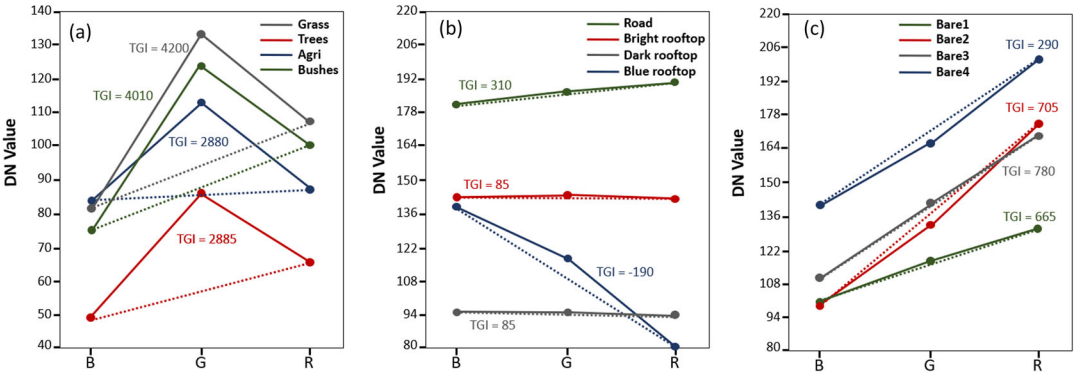

Figure 5. TGI for different land covers: (a) vegetation; (b) roads and rooftops; (c) bareland.

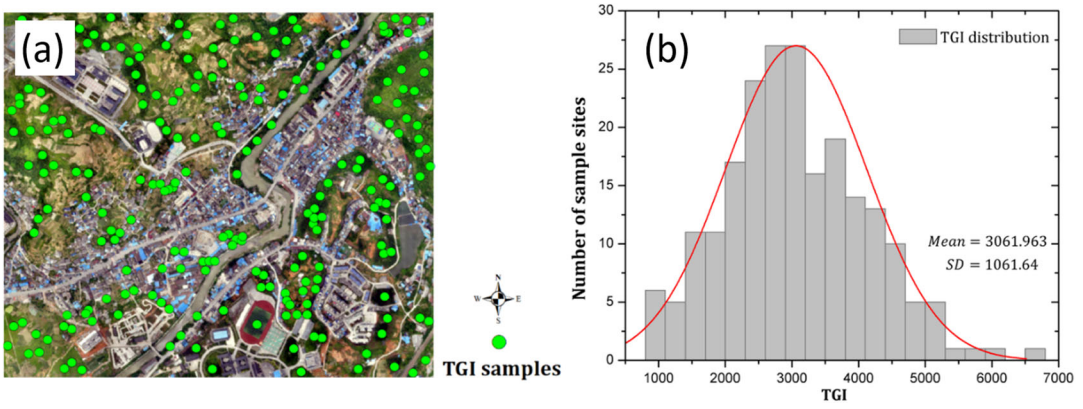

Figure 6. TGI samples sites (a) and TGI distribution (b).

SD_{tgi}, is 1061.64. The range of 2 times of SD_{tgi} from the mean, [938.38 – 5185.24], covering over 95 percent of the samples. A pixel with high TGI has a high probability of being vegetation.

One of the limitations of TGI is that it may misclassify other objects with a similar triangle-area as vegetation. For example, yellow objects (such as dry, bright bareland) have a similar TGI value with vegetation. Figure 7 shows that not only vegetation but also the yellow parking line has a high TGI value. Figure 7 (a.1) and (b.1) are the original images, and the green mask in Figure 7(a.2) and (b.2) are the pixels with TGI larger than 938. The yellow line of the parking lot and the dry bareland with a bright yellow color were mislabeled as vegetation. This drawback can be improved by limiting the DN values of a pixel under 120 when calculating TGI. Figure 7(c) shows the triangles of the yellow lines and the vegetation both have the same area, a TGI of 3,000. The triangle of yellow lines is higher than the vegetation in the "DN value" axis, so we restricted the triangle in the low position (all DN values lower than 120) of the Wavelength-DN plot to get a reliable TGI threshold for vegetation.

After calculating the TGI value of each low tone pixel in $TDOM_B$, we used the polygons of changed areas derived from ΔDSM to conduct zonal statistics on TGI raster, then marked out the polygons with a TGI mean less than 938 as non-vegetation changed areas.

Extraction of building changes

We utilized several parameters to extract the changed buildings from the non-vegetation changes. In the study area, the average height of a story is about 2 to 3 m. Hence, we removed minor

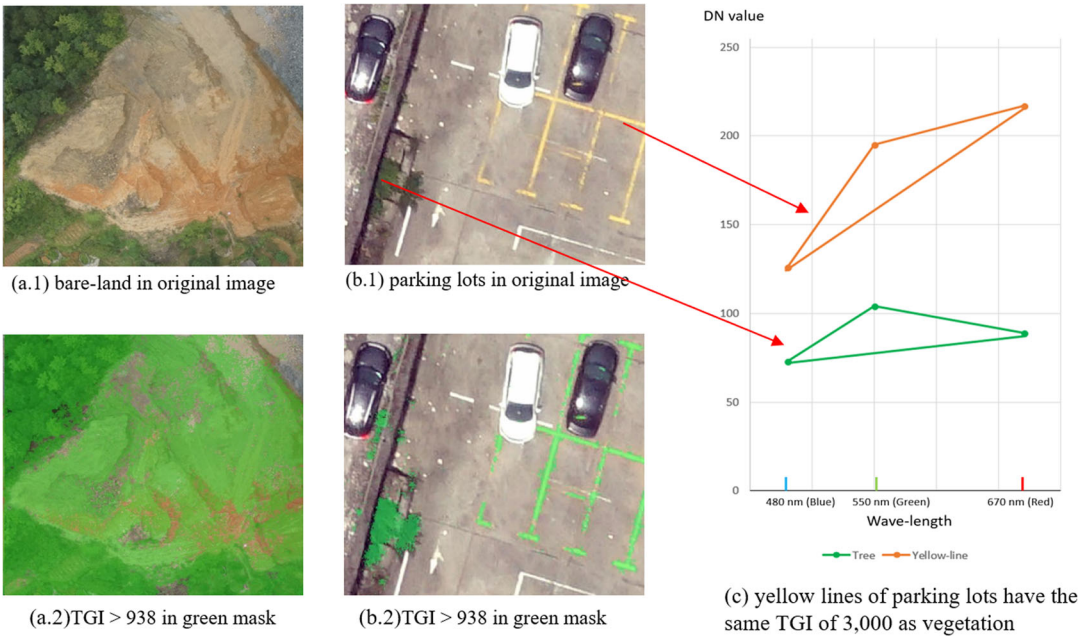

Figure 7. The highlighted yellow tone in images has a similar TGI as vegetation.

changes less than 2 m to eliminate changes from vehicles and other small objects. Then the change areas were reclassified into two classes: changed (>2 m) and non-changed (other values).

A size threshold, T_s, was further utilized to filter out small-size polygons. We set T_s to be 9 m^2 (3 m × 3 m), the smallest size that a building can be habitable. Additionally, we noticed that the image matching algorithm tends to cause many banded sliver polygons next to the edge of the buildings. To solve this problem, we designed a simple method by calculating the width of the approximate rectangle. This rectangle is assumed to have the same area and perimeter of a changed polygon. The width (w) of the approximate rectangle is calculated by:

$$w = \frac{P}{4} - \sqrt{\frac{P^2}{16} - A} \tag{2}$$

where P and A denote the perimeter and the area of a changed polygon, respectively. Equation (2) is derived from $P = 2 \times (w + h)$ and $A = w \times h$, where h is the height of the approximate rectangle. We removed the small banded sliver polygons with a w smaller than 1 m. Table 1 lists several examples of the removed banded sliver polygons.

Results

Registration of DSM and TDOM

The aero-triangulation procedure successfully processed two epochs of images in a single project, and it matched 1.25 million tie points with 4.72 million tie point observations. Each image has about 3000 tie point observations on average. The RMS of tie points is 1.08 pixels. A DSM with 0.16 m resolution (Figure 8) and a TDOM with 0.05 m resolution were generated for each epoch. The RMSE (Root Mean Square Error) of the two DSMs is 0.123 m, and the mean value is about 0 (Figure 9). Thus there is no significant systematic bias between the two DSMs, and the ΔDSM can reflect the elevation changes caused by new stories (usually > 2 m). Figure 10 presents some topical scenes in the study area, which demonstrate that TDOMs align each other well with an error of 1 pixel (0.05 m).

Table 1. Examples of the removed banded sliver polygons.

Banded sliver polygon	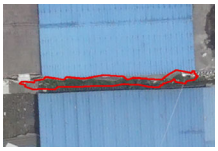			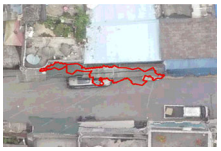
Area (m^2)	9.26	10.17	9.00	12.51
Perimeter (m)	30.26	28.63	22.53	37.94
h (m)	14.49	13.56	10.55	18.28
w (m)	0.64	0.75	0.95	0.68
Approximate rectangle				

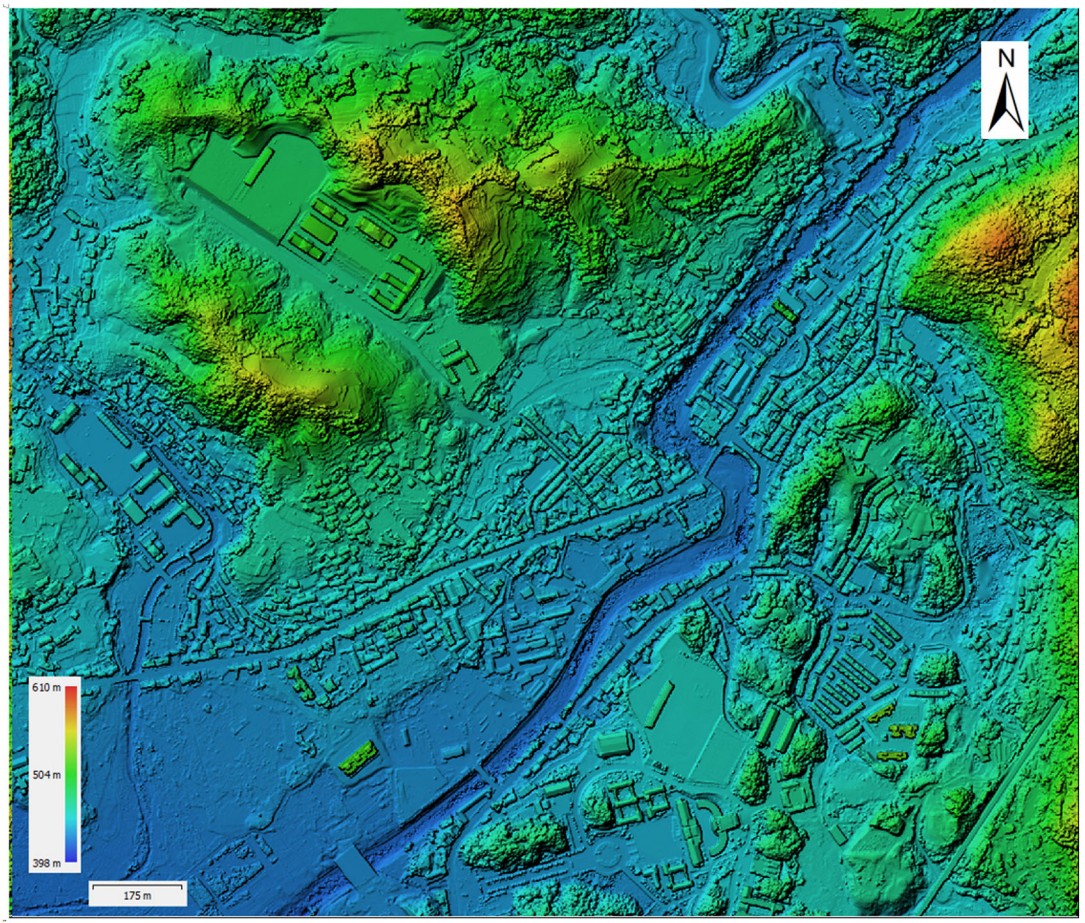

Figure 8. The DSM_B extracted from the sUAS image.

Error assessment of change detection

The changes areas derived from ΔDSM was converted to a vector file which contains 1.04 million polygons, 5,094 of which were larger than 9 m^2, the improved TGI labeled 4,690 polygons as vegetation, and only 12 non-green trees were left. About half of the remaining 404 polygons were removed due to their small widths (<1 m), see Figure 11 About half of the non-vegetation changed areas have a width of less than 1 m. After applying multiple criteria described in Section

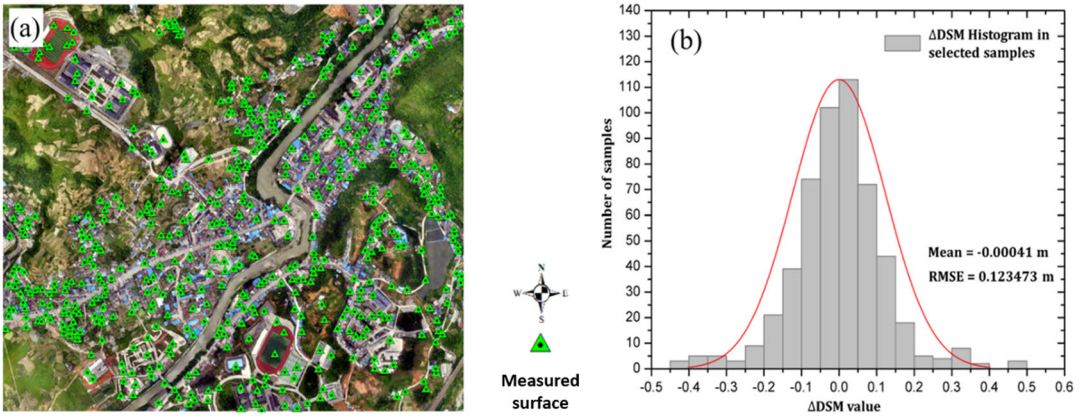

Figure 9. ΔDSM accuracy assessment: (a) locations of measured hard flat surfaces. (b) statistics of ΔDSM values of measured surfaces.

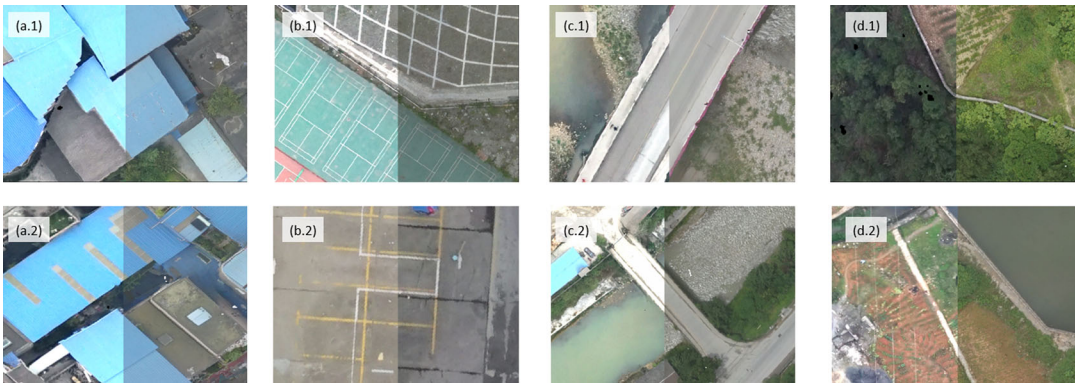

Figure 10. $TDOM_A$ and $TDOM_B$ align each other well within 1 pixel. The right part of each image comes from $TDOM_{A,}$ and the left comes from $TDOM_B$.

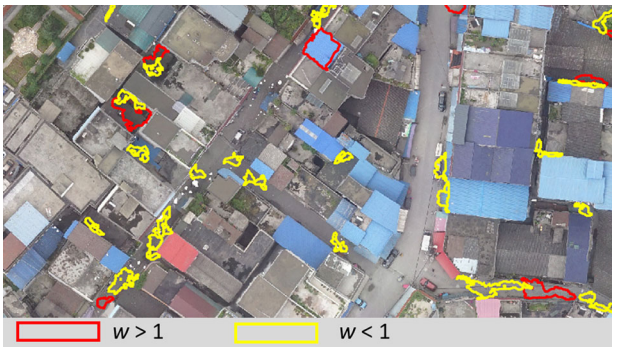

Figure 11. About half of the non-vegetation changed areas have an approximate width of less than 1 m.

Extraction of building changes, the workflow extracted 97 changed areas as positive. 36 out of 97 were true positives, covering 28 of 30 ground truth polygons. Only two changed buildings were not detected (6.7 percent). The false matched DSM and large trucks cause most of the false detections. The customized ArcGIS Pro Toolbox took 5 minutes to extract those 97 changes polygons based on the DSMs and TDOMs in a computer with one Intel i7-8700K CPU. In comparison, it took an operator 3.5 hours to extract the ground truth manually.

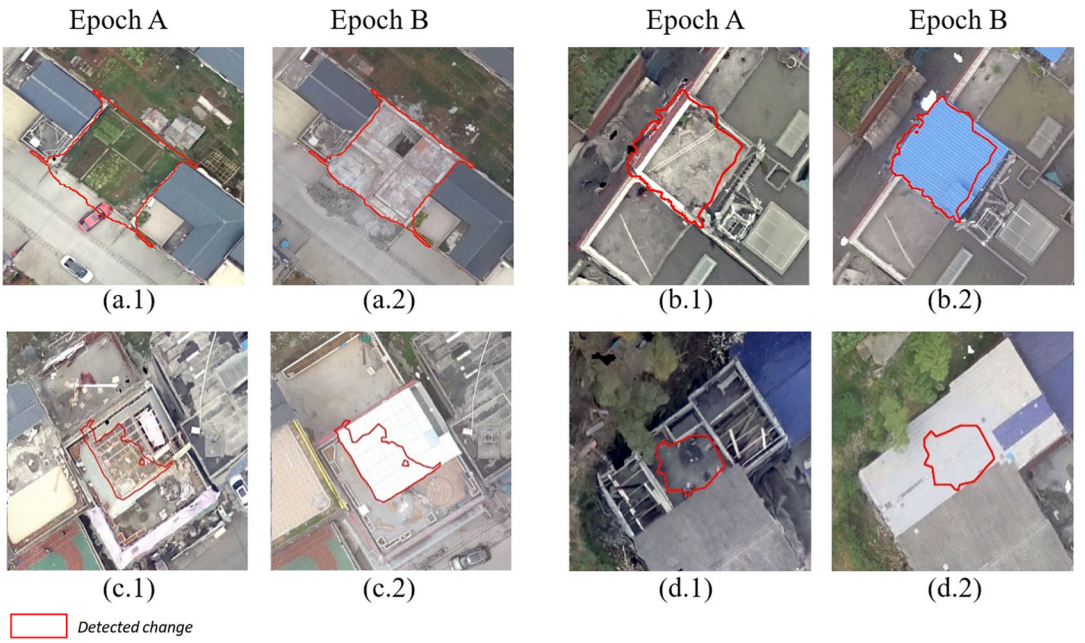

Figure 12. Examples of true positives.

Most true positives are the new stories or structures added to the existing buildings. Figure 12 illustrates four typical examples of true positive, including new buildings and structures. Figure 12 (a.2) shows a new 17 m-high building on the site of Figure 12 (a.1). Figure 12 (b.2) displays a 3 m-high new shed on the building in Figure 12 (b.1). Two buildings in Figure 12 (c.2) and Figure 12 (d.2) have been heightened by 3 m than Figure 12 (c.1) and 12 (d.1), respectively, indicating that potentially a new story has been added between the two epochs. The changed areas in Figure 12 (c.2) and (d.2) seem not to be fully detected because only a part of the building increased over 2 m.

Figure 13 shows two successfully detected changes, and even they are difficult to be discovered by the naked eye. Figure 13 (a.2) shows an 11 m high new, small building on the site of Figure 13 (a.1) where is messy and difficult to judge whether there is a building in this densely built community. The building in Figure 13 (b.2) is 6 m higher than the same building in Figure 13 (b.1), indicating that two stories were added. This change cannot be detected by the naked eye reliably. Carefully observation on the bird's eye images Figure 13 (b.3) and (b.4) verifies the significate change of the building's height.

61 polygons are misclassified as changed buildings (false positives). Figure 14 presents six causes of these errors. 17 pseudo changes are caused by false DSM from the image matching algorithm of PhotoScan, and another 15 changes are caused by the movements of large trucks with heights more than 3 m. The growth of trees makes up 12 errors, which are not "green" enough, and have low TGIs less than 938. The new awning, mound, and construction materials lead to 17 false detections.

Figure 15 presents the only two missed changes. The new blue shed in Figure 15 (a.2) was ignored as the width of its approximate rectangle is less than 1 m. We also noticed that the image matching algorithm proves less effectiveness in valleys due to shadow and occlusion. Few tie points can be matched in the valley. In Figure 15 (b.2), a new shed was ignored because only a small part in its edge was raised over 2 m and this part was merged with a tree next to it. This mistakenly merged polygon was labeled as vegetation due to its high TGI value and then was removed.

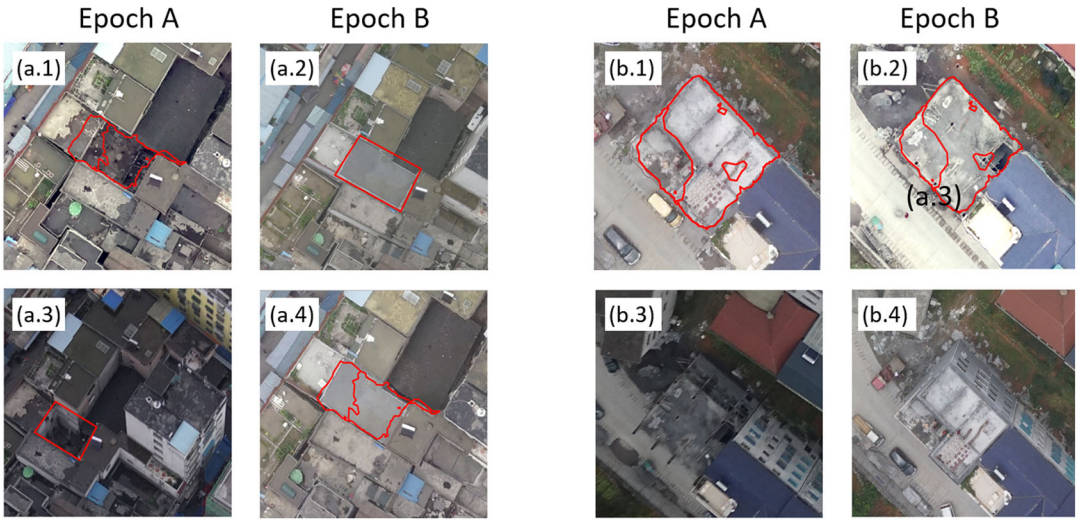

Figure 13. Two examples of new construction with little textural changes. (a.2) shows an 11 m high new building on the site of (a.1). Bird's eye image (a.3) and (a.4) visually prove the detection. The building in (b.2) is 6 m higher than the same building in (b.1), indicating that two stories were added. This change is hard to find by the naked eye in TDOMs and bird's eye images.

Figure 14. Causes of false detection.

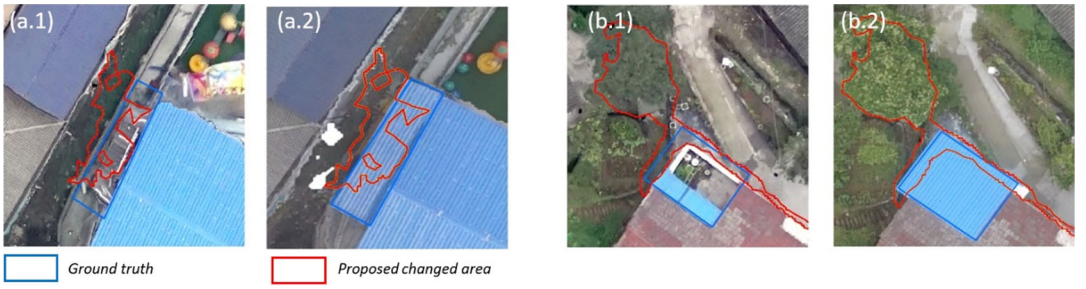

Figure 15. The two changed buildings not detected. In each pair, the right image is the newer epoch.

Discussion

The proposed workflow based on sUAS images alone has a high recall for building change detection and can detect the new stories added on existing buildings. It uses the discrepancy of two DSMs and an improved TGI to detect changed buildings. The workflow is simple since

unnecessary processes (geo-referencing and measuring control points) are reduced, and no extra data or particular sensors (*e.g.*, LiDAR or multispectral sensor) are needed.

In the study case, most changed buildings are detected, including the new structure added to the existing building. This sensibility comes from the high relative accuracy of two DSMs, which is critical in vertical change detection. The elevation change capability was quantitatively given by the accuracy assessment of ΔDSM. The RMSE of ΔDSM is 0.123, meaning that most of the added structure with more than two times of RMSE can be detected.

About 63 percent detections are false, majorly due to the intrinsic flaw in the image matching algorithm in PhotoScan and the complex urban environment. However, this method is practically feasible because the false detections only require several minutes to be manually removed, which is a considerable advantage compared with the time-consuming field visits or visual interpretation.

Traditionally, registering two datasets of aerial images needs to conduct aero-triangulation for each epoch with common GCPs. The orthoimages from this strict solution are registered to a spatial coordinate system and aligned to other rectified geographic data. However, measuring GCP in the field is costly in terms of labor and finance. Introducing GCPs into aero-triangulation is also time- and labor-intensive. In our research, the images from two epochs are processed in a single aero-triangulation procedure, and the registration is accomplished simultaneously. No GCP measuring is needed. The DOMs have approximate coordinates from navigating the GPS device of the sUAS, and may have location error. However, this error is acceptable in practice. The local law enforcement more concerns about rapid situation awareness of illegal constructions and then goes to those scenes to verify them. The concise workflow used in this research helps reducing costs in the circumstance of no accurate location is required.

TGI, which takes the area of the triangle formed by DN values of a pixel in visual bands as an indicator for vegetation. TGI is a linear combination of RGB bands, so it potentially causes information loss because that three DN values are compressed to a number. As compensation, we add a constraint on the DN value of RGB bands: only pixels in the low tone (DN $<$120) need to compute TGI. This restriction is based on the low reflection of vegetation in the optical spectrum.

The study area covers the entire town and is several times larger than other relevant studies (Li et al. 2017; Qin 2014). The rich texture and various objects within this large area well tested the advantages and drawbacks of the proposed method. The moving object, such as trucks and awnings, have not been reported in the current literature on building change detection. Benefiting from the sufficient size of the study area, the hinder of those objects is revealed. The number of changed buildings is more than the small areas the previous research (Li et al. 2017; Qin 2014), so that universality and reproducibility of the proposed method is well verified by the high recall.

The proposed approach takes 5 minutes to monitor 2 km^2 urban area, while the traditional manual method (piece by piece) is 42 times slower ($\sim$3.5 hours). This advantage of speed tends to be more noticeable when monitoring a large area, for example, monitoring several towns simultaneously. Given the rapid feedback, the user can also test different parameters, such as the TGI threshold for vegetation, to attain the most credible result. Although the proposed method tends to produce many false detections, those false detections can be easily removed through a quick manual inspection. In this situation, the advantages of the proposed method overweigh its disadvantages.

The width of the approximate rectangle of the changed polygon is used to remove the banded sliver areas caused by incorrect edges of buildings in DSM. This approach can be easily applied to other applications. For example, the ratio of width and length can be used to check whether a polygon is a road polygon or not in the land-use domain.

While the results are promising, the proposed approach can be improved from the following aspects. From the spectral viewpoint, urban sUAS images have several characteristics in visible

spectrum: 1) human-made objects tend to have a relatively high reflectance, especially in the red or blue band, and 2) natural objects tend to have relatively low reflectance (like vegetation). Further researches are needed to explore the spectral feature space between different objects in sUAS images. In addition, TGI is designed for the reflectance of visible remote sensing images, and errors will be introduced when DN values are used instead of calibrated reflectance. More research is needed to identify the relationship between DN value and reflectance better.

The image matching algorithm plays a key role in the proposed method. Point cloud generating methods may fail in some objects with less texture, such as water bodies. In addition, it is challenging to exclude trucks via structure and textural information as their height and size are similar to small buildings. Similarly, new construction materials, mounds, and awnings have caused false detections.

Other data sources would benefit high-resolution detection for building change. Though bringing higher cost, 3D-reconstruction based on oblique imagery can provide more details than nadir imagery. To better identify vegetation, infrared sensors would be preferred in some circumstances. Compared with sUAS images, satellite images, even with a resolution of 0.3 m, lacks flexibility and rapid response to some degree. In addition, the generation of detailed DSM is a disadvantage of satellite imagery.

Limitations

In this study, most changed buildings are detected. The intrinsic flaw in the image matching algorithm and the complex urban environment cause most of the false detections. However, this method is practically feasible because the false detections only require several minutes to be manually removed, which is a considerable advantage compared with the time-consuming field visits or visual interpretation. Nevertheless, its limits should be recognized before applying to other scenarios. The parameters used for the study area may not be general, especially the TGI threshold of vegetation, as well as the low tone threshold. These two values vary according to image quality. Other vegetation indices may face the same challenge when facing images with poor quality. The minimum detecting area, elevation height, and approximate width can be adjusted according to the requirements of users.

The registration of two epochs in a single aero-triangulation is applicable in short time interval monitoring. If the time interval is too long (*e.g.*, 12 months), the earth surface may change largely, thus the image matching algorithm may fail to find tie points between two epochs. In that case, each epoch should be processed individually, and then conduct registration.

Another notable limitation of the proposed approach is that the absence of building detection algorithms leads to mingled results of buildings and non-buildings (*e.g.*, trucks and trees). Vegetation index such as TGI or Excess Green minus Excess Red (ExG - ExR) (Meyer and Neto 2008) can eliminate the vegetation growth in ΔDSM, but it is not feasible to develop algorithms individually for each type of non-building objects.

Conclusion

The proposed method uses elevation, color, and shape information derived from the sUAS images to efficiently detect new buildings and added structures to existing buildings. In short time interval monitoring, new structures to existing buildings, rather than complete new buildings from the ground up, consist of most of the changes (87 percent) in the study area.

Images from two epochs are integrated by a single aero-triangulation procedure, which minimizes the aligning error of two DSMs and provides high relative accuracy for horizontal and vertical change detection. According to the quantitative analysis of its accuracy (RSME = 0.123 m),

the ΔDSM can detect small added structures. The one aero-triangulation procedure requires no ground control points, which significantly reduces the workload of the in-field survey.

The modified TGI index has been proved efficient in removing natural changes such as vegetation phenological variation. The approximate width of the changed polygon is effective in eliminating banded sliver polygons resulted from the deficient image matching algorithms.

Image matching algorithms and large moving objects (*e.g.*, trucks) caused most of the false detections. However, the high recall (93.3 percent) guarantees that most building changes. Several types of false detection were elaborated in this paper, providing valuable information for further research and applications. The approach developed in this study is simple and practical, and it aids users in obtaining new buildings and added structures. It could be applied to a larger geographic extent to assist people in urban planning and decision making.

ORCID

Xiao Huang http://orcid.org/0000-0002-4323-382X
Zhenlong Li http://orcid.org/0000-0002-8938-5466
Cuizhen Wang http://orcid.org/0000-0002-0306-9535

References

Awrangjeb, M., M. Ravanbakhsh, and C. S. Fraser. 2010. Automatic detection of residential buildings using LIDAR data and multispectral imagery. *ISPRS Journal of Photogrammetry and Remote Sensing* 65 (5):457–67. doi: 10.1016/j.isprsjprs.2010.06.001.

Baltsavias, E. P. 1999. A comparison between photogrammetry and laser scanning. *ISPRS Journal of Photogrammetry and Remote Sensing* 54 (2–3):83–94. doi: 10.1016/S0924-2716(99)00014-3.

Champion, N. 2007. 2D building change detection from high resolution aerial images and correlation digital surface models. *International Archives of Photogrammetry, Remote Sensing and Spatial Information Sciences* 36 (3/W49A):197–202.

Champion, N., F. Rottensteiner, L. Matikainen, X. Liang, J. Hyyppä, and B. P. Olsen. 2009. A test of automatic building change detection approaches. Proceedings of CMRT09 03–4.

Chen, B., Z. Chen, L. Deng, Y. Duan, and J. Zhou. 2016. Building change detection with RGB-D map generated from UAS images. *Neurocomputing* 208 (October):350–64. doi: 10.1016/j.neucom.2015.11.118.

Chen, L.-C., and L.-J. Lin. 2010. Detection of building changes from aerial images and light detection and ranging (LIDAR) data. *Journal of Applied Remote Sensing* 4 (1):041870. doi: 10.1117/1.3525560.

Colomina, I., and P. Molina. 2014. Unmanned aerial systems for photogrammetry and remote sensing: a review. *ISPRS Journal of Photogrammetry and Remote Sensing* 92 (June):79–97. doi: 10.1016/j.isprsjprs.2014.02.013.

Deng, J. S., K. Wang, Y. Hong, and J. G. Qi. 2009. Spatio-temporal dynamics and evolution of land use change and landscape pattern in response to rapid urbanization. *Landscape and Urban Planning* 92 (3-4):187–98. doi: 10.1016/j.landurbplan.2009.05.001.

Hermosilla, T., L. A. Ruiz, J. A. Recio, and J. Estornell. 2011. Evaluation of automatic building detection approaches combining high resolution images and LiDAR data. *Remote Sensing* 3 (6):1188–210. doi: 10.3390/rs3061188.

Hodgson, M. E., and P. Bresnahan. 2004. Accuracy of airborne Lidar-derived elevation. *Photogrammetric Engineering & Remote Sensing* 70 (3):331–9. doi: 10.14358/PERS.70.3.331.

Hunt, E. R., P. C. Doraiswamy, J. E. McMurtrey, C. S. T. Daughtry, E. M. Perry, and B. Akhmedov. 2013. A visible band index for remote sensing leaf chlorophyll content at the canopy scale. *International Journal of Applied Earth Observation and Geoinformation* 21 (April):103–12. doi: 10.1016/j.jag.2012.07.020.

Hussain, M., D. Chen, A. Cheng, H. Wei, and D. Stanley. 2013. Change detection from remotely sensed images: from pixel-based to object-based approaches. *ISPRS Journal of Photogrammetry and Remote Sensing* 80:91–106. doi: 10.1016/j.isprsjprs.2013.03.006.

Ioannidis, C., C. Psaltis, and C. Potsiou. 2009. Towards a strategy for control of suburban informal buildings through automatic change detection. *Computers, Environment and Urban Systems* 33 (1):64–74. doi: 10.1016/j.compenvurbsys.2008.09.010.

Kršák, B., P. Blišťan, A. Pauliková, P. Puškárová, Ľ. Kovanič, J. Palková, and V. Zelizňaková. 2016. Use of low-cost UAS photogrammetry to analyze the accuracy of a digital elevation model in a case study. *Measurement* 91 (September):276–87. doi: 10.1016/j.measurement.2016.05.028.

Li, W., K. Sun, D. Li, T. Bai, and H. Sui. 2017. A new approach to performing bundle adjustment for time series UAS images 3D building change detection. *Remote Sensing* 9 (6):625. doi: 10.3390/rs9060625.

Liu, X. 2011. Accuracy assessment of lidar elevation data using survey marks. *Survey Review* 43 (319):80–93. doi: 10.1179/003962611X12894696204704.

Liu, Y., F. Fang, and Y. Li. 2014. Key issues of land use in china and implications for policy making. *Land Use Policy* 40 (September):6–12. doi: 10.1016/j.landusepol.2013.03.013.

Maiti, S. K. 2013. Topsoil management. In *Ecorestoration of the coalmine degraded lands*, 83–96. India: Springer. doi: 10.1007/978-81-322-0851-8_5.

Matikainen, L., J. Hyyppä, E. Ahokas, L. Markelin, and H. Kaartinen. 2010. Automatic detection of buildings and changes in buildings for updating of maps. *Remote Sensing* 2 (5):1217–48. doi: 10.3390/rs2051217.

Meyer, G. E., and J. C. Neto. 2008. Verification of color vegetation indices for automated crop imaging applications. *Computers and Electronics in Agriculture* 63 (2):282–93. doi: 10.1016/j.compag.2008.03.009.

Nex, F., and F. Remondino. 2014. UAS for 3D mapping applications: a review. *Applied Geomatics* 6 (1):1–15. doi: 10.1007/s12518-013-0120-x.

Qin, R. 2014. An object-based hierarchical method for change detection using unmanned aerial vehicle images. *Remote Sensing* 6 (9):7911–32. doi: 10.3390/rs6097911.

Qin, R., J. Tian, and P. Reinartz. 2016. 3D change detection – approaches and applications. *ISPRS Journal of Photogrammetry and Remote Sensing* 122 (December):41–56. doi: 10.1016/j.isprsjprs.2016.09.013.

Qin, R., X. Huang, A. Gruen, and G. Schmitt. 2015. Object-based 3-D building change detection on multitemporal stereo images. *IEEE Journal of Selected Topics in Applied Earth Observations and Remote Sensing* 8 (5):2125–37. doi: 10.1109/JSTARS.2015.2424275.

Shalaby, A., and R. Tateishi. 2007. Remote sensing and GIS for mapping and monitoring land cover and land-use changes in the Northwestern Coastal Zone of Egypt. *Applied Geography* 27 (1):28–41. doi: 10.1016/j.apgeog.2006.09.004.

Stal, C., F. Tack, P. De Maeyer, A. De Wulf, and R. Goossens. 2013. Airborne photogrammetry and Lidar for DSM extraction and 3D change detection over an urban area–a comparative study. *International Journal of Remote Sensing* 34 (4):1087–110. doi: 10.1080/01431161.2012.717183.

Sui, H., J. Tu, Z. Song, G. Chen, and Q. Li. 2014. A novel 3D building damage detection method using multiple overlapping UAS images. In *The International Archives of Photogrammetry, Remote Sensing and Spatial Information Sciences; Gottingen*, XL:173–9. Gottingen, Germany, Gottingen: Copernicus GmbH. doi: 10.5194/isprsarchives-XL-7-173-2014.

Szabó, S.,. L. Bertalan, Á. Kerekes, and T. J. Novák. 2016. Possibilities of land use change analysis in a mountainous rural area: a methodological approach. *International Journal of Geographical Information Science* 30 (4):708–26. doi: 10.1080/13658816.2015.1092546.

Tian, J., S. Cui, and P. Reinartz. 2014. Building change detection based on satellite stereo imagery and digital surface models. *IEEE Transactions on Geoscience and Remote Sensing* 52 (1):406–17. doi: 10.1109/TGRS.2013.2240692.

Tong, X., Z. Hong, S. Liu, X. Zhang, H. Xie, Z. Li, S. Yang, W. Wang, and F. Bao. 2012. Building-damage detection using pre- and post-seismic high-resolution satellite stereo imagery: a case study of the May 2008 Wenchuan earthquake. *ISPRS Journal of Photogrammetry and Remote Sensing* 68 (March):13–27. doi: 10.1016/j.isprsjprs.2011.12.004.

Unger, J., M. Reich, and C. Heipke. 2014. UAS-based photogrammetry: monitoring of a building zone. *ISPRS - International Archives of the Photogrammetry, Remote Sensing and Spatial Information Sciences* 40 (5):601. doi: 10.5194/isprsarchives-XL-5-601-2014.

Verhoeven, G. 2011. Taking computer vision aloft – archaeological three-dimensional reconstructions from aerial photographs with photoscan. *Archaeological Prospection* 18 (1):67–73. doi: 10.1002/arp.399.

Weng, Q. 2002. Land use change analysis in the Zhujiang delta of china using satellite remote sensing, GIS and stochastic modelling. *Journal of Environmental Management* 64 (3):273–84. doi: 10.1006/jema.2001.0509.

Xuan, W. 2011. Topographical change detection from UAS imagery using M-DSM method. In *Applied Informatics and Communication*, 596–605. Berlin, Heidelberg: Communications in Computer and Information Science, Springer. doi: 10.1007/978-3-642-23223-7_77.